

Published in final edited form as:

Nat Cell Biol. 2008 January 01; 10(1): 30–41. doi:10.1038/ncb1666.

ARF1 is directly involved in dynamin-independent endocytosis

Sudha Kumari¹, Satyajit Mayor^{1,2}

¹National Centre for Biological Science (TIFR), Bellary Road, , Bangalore 560 065, India.

Abstract

Endocytosis of glycosylphosphatidyl inositol (GPI)-anchored proteins (GPI-APs) and the fluid phase takes place primarily through a dynamin- and clathrin-independent, Cdc42-regulated pinocytic mechanism. This mechanism is mediated by primary carriers called clathrin-independent carriers (CLICs), which fuse to form tubular early endocytic compartments called GPI-AP enriched endosomal compartments (GEECs). Here, we show that reduction in activity or levels of ARF1 specifically inhibits GPI-AP and fluid-phase endocytosis without affecting other clathrin-dependent or independent endocytic pathways. ARF1 is activated at distinct sites on the plasma membrane, and by the recruitment of RhoGAP domain-containing protein, ARHGAP10, to the plasma membrane, modulates cell-surface Cdc42 dynamics. This results in the coupling of ARF1 and Cdc42 activity to regulate endocytosis at the plasma membrane. These findings provide a molecular basis for a crosstalk of endocytosis with secretion by the sharing of a key regulator of secretory traffic, ARF1.

Internalization of cargo at the cell surface takes place via multiple clathrin-dependent and independent pathways^{1–3}. Many of these mechanisms use the large GTPase dynamin to facilitate vesicle fission at the plasma membrane, although other pathways function in its absence. A dynamin-independent, Cdc42-regulated pinocytic pathway is one such example⁴; it does not use the coat-proteins, caveolin or clathrin, nor the scission effector, dynamin. Nascent endocytic vesicles (CLICs) in this pathway have been recently identified⁵, and they fuse to form early endosomal intermediates, GEECs⁴. This is distinct from the early sorting endosomal compartment which also contains clathrin-dependent endocytic cargo⁶. Although the GEEC pathway is responsible for endocytosis of specific components of the membrane such as GPI-APs and cholera toxin (CTx) bound to its ganglioside receptor (GM1), it also facilitates pinocytosis in a variety of cell lines^{4–8}.

Recently, we have shown that cholesterol-sensitive Cdc42 activation results in recruitment of actin-polymerization machinery to specific foci at the plasma membrane, promoting endocytosis via CLICs into GEECs⁹. This results in an endocytic pathway that is sensitive to perturbations of cholesterol levels and actin polymerization. To date, very few other components of this pathway have been identified. Flotillin1 has been reported to be required for internalization via a clathrin and dynamin independent pathway¹⁰, and CtBP1–BARS protein has been implicated in a dynamin-independent pinocytic mechanism¹¹. Further

²Correspondence should be addressed to S.M. (mayor@ncbs.res.in).

AUTHOR CONTRIBUTIONS

S.K. executed and analysed all experiments. S.K. and S.M. planned all experiments and wrote the manuscript.

downstream, Rab5 and PI(3)K are recruited to early endocytic intermediates of the GEEC pathway, resulting in fusion with sorting endosomes⁶.

The functional significance of endocytosis via GEECs is expanding as we discover both specific cargo and molecular players that participate in this pathway; for example, folate uptake via GPI-anchored folate receptors (FR-GPI), and the internalization of vacuolating toxins such as VacA and aerolysin, are mediated by this pathway^{3,12}. Taking into account the diverse functions of GPI-AP cargo and the importance of fluid-phase endocytosis for a variety of cellular processes, it is imperative to understand the molecular mechanism of the GEEC pathway.

Here, we have examined the role of the ADP-ribosylation factor (ARF) family of proteins that participate in multiple intracellular trafficking events¹³. Of the many family members¹³, ARF1 and ARF6 are the best characterized. ARF1 has a central role in vesicle formation during early and late secretory traffic^{14,15}, whereas ARF6 is involved in regulating the actin cytoskeleton near the cell surface and has been implicated in multiple pathways of endocytosis^{16–8}. We find that activated ARF1 is present at the plasma membrane and recruits ARHGAP10, a GAP for Cdc42, which, in turn, regulates endocytosis via the GEEC pathway.

Results

Modulation of ARF1 GTPase activity specifically affects endocytosis via the GEEC pathway

ARF1, a cytosolic GTPase with a relative molecular mass of 21,000 (M_r , 21K), is recruited to Golgi membranes, where its location in the membrane depends on GTP-binding¹⁹. The GDP-exchange deficient form of ARF1 (ARF1^{T31N}) is primarily cytosolic, and behaves as dominant negative isoform of ARF1 activity when overexpressed²⁰. To study the effect of ARF1 on different pathways of endocytosis, uptake of endocytic cargo specific for each pathway in ARF1^{T31N}-overexpressing CHO cells was quantitatively assessed (Fig. 1a). Endocytosis via the dynamin-dependent pathways, clathrin, caveolin or the RhoA-dependent processes were monitored by measuring the extent of endocytosis of fluorescently-labelled transferrin (Tf) bound to the transferrin receptor (TfR), C₆-Bodipy-lactosylceramide (C₆-LacCer) incorporated into the plasma membrane, or antibodies against the β -subunit of the interleukin 2 receptor (IL2R- β)²¹, respectively. Endocytosis via the GEEC pathway was assessed by monitoring uptake of surface-labelled folate receptor (FR-GPI) and TMR-labelled Dextran (TMR-Dex), as probes for GPI-APs and the fluid-phase, respectively. Overexpression of ARF1^{T31N} resulted in specific inhibition of FR-GPI and TMR-Dex uptake, whereas internalization of Tf (Fig. 1a) and C₆-LacCer (see Supplementary information, Fig. S1a) were unaffected. Although ARF1^{T31N} caused a reduction in the surface levels of the IL2R- β , possibly due to its effect on IL2R- β exocytosis, endocytosis of IL2R- β was also unaffected (see Supplementary information, Fig. S1d).

The effect of ARF1^{T31N} on the CLIC-GEEC pathway was not restricted to CHO cells. ARF1^{T31N} expression inhibited FR-GPI and fluid-phase uptake in BHK cells (see Supplementary information, Fig. S2a), and the uptake of GEEC cargo, CTxB and

fluid-phase in mouse embryonic fibroblasts (MEFs; Fig. 1b)^{5,6}. In cells overexpressing ARF1^{T31N}, steady-state levels of surface FR–GPI were increased (see Supplementary information, Fig. S2c), consistent with inhibition of GPI-AP endocytosis. ARF1 also plays a role in GPI-AP exocytosis, as surface delivery of GPI-APs (see Supplementary information, Fig. S2b) was also inhibited. In parallel, there was a reduction in surface levels of TfR (see Supplementary information, Fig. S2d), and together with alteration in morphology of TfR containing perinuclear-recycling compartment (Fig. 1a), these results suggest a role for ARF1 in the exocytosis of TfR and in TfR recycling²².

ARF1 depletion inhibits uptake via the GEEC pathway

ARF1^{T31N} overexpression could inhibit endocytosis via GEECs by sequestering GDP exchange factors (GEFs) for other ARF family members, besides ARF1, as some GEFs have overlapping specificity for ARF1 and ARF6 (ref. 23). To discount this possibility, ARF1 protein was depleted using RNA interference (RNAi) methodology²². Approximately 60 h post-transfection with *ARF1*-specific short hairpin RNA (shRNA), cells appeared morphologically distinct (see Supplementary information, Fig. S2e) and ARF1 protein levels were reduced (Fig. 2b). The differences in actin levels observed between control and shRNA-transfected cells may have resulted from the unequal number of cells loaded in different lysates. Although surface-receptor normalized Tf-uptake was unaffected, FR–GPI and the fluid-phase uptake were markedly reduced (Fig. 2a, c and d). Similar results were observed with another shRNA sequence against *ARF1* (data not shown). A reduction in fluid-phase uptake by ARF1 shRNA-treated cells was also confirmed by a biochemical assay, using horseradish peroxidase (HRP) as a fluid-phase probe (Fig. 2e).

ARF1 depletion decreased both the number of fluid-containing endosomes and average endosomal intensities (see Supplementary information, Fig. S3a, b and c). Furthermore, reduction in FR–GPI uptake after treatment with ARF1 shRNA was not due to decreased cell-surface levels, as FR–GPI endocytosis was reduced in ARF1 depleted cells at comparable surface levels of FR–GPI (Fig. 2d). Similarly to results obtained with ARF1^{T31N} expression, ARF1 depletion caused a reduction in cell-surface levels of TfR, consistent with previous studies on the role of ARF1 in membrane recycling to the plasma membrane^{22,24}. In ARF1-depleted cells, there was a detectable reduction in ARF3 levels (Fig. 2b). As the ARF1 target sequences do not share any significant sequence similarity with ARF3, this could be a result of coregulation of the protein products in CHO cells; however, further experiments are required to confirm this possibility. To directly test the involvement of ARF3, cells were transfected with shRNA against *ARF3* (Fig. 2a, c) and endocytosis was measured. In ARF3-depleted cells, ARF3 levels were reduced without altering ARF1 levels (Fig. 2b); however, there was no reduction in fluid-phase, TfR or FR–GPI uptake (Fig. 2a, c). Similarly in cells depleted of ARF4 or ARF5, there was no detectable reduction in fluid uptake (see Supplementary information, Fig. S4). Moreover, expression of an RNAi-resistant form of ARF1 (Fig. 3a) that rescues the levels of ARF1 protein (Fig. 3c, d) restored fluid-phase uptake significantly (Fig. 3b). In cells transfected with ARF1 shRNA, Golgi morphology was altered to a more hazy appearance. Consistent with rescue of ARF1 function, the morphology of the Golgi was also restored in cells expressing the RNAi-resistant construct when cotransfected with shRNA against *ARF1* (Fig. 3e). In

contrast, depletion of ARF6 by shRNA did not affect endocytosis via the GEEC pathway (see Supplementary information, Fig. S3d). These results provide evidence that ARF1 is specifically required for endocytosis via the GEEC pathway.

Involvement of ARF1 in the GEEC pathway is distinct from its role in secretion

Recently, perturbation of Syntaxin6 function was shown to inhibit caveolar uptake in human foreskin fibroblasts via inhibition of delivery of specific membrane components from the Golgi²⁵. One explanation for the inhibition of endocytosis is an indirect effect by inhibition of membrane traffic from the Golgi to the plasma membrane, as perturbation of ARF1 inhibits Golgi-to-cell surface delivery of GPI-APs and other cargo^{22,26,27} (see Supplementary information, Fig. S2b). Many secretory mutants in yeast are also known to have endocytic defects²⁸. To test this hypothesis, cells were treated with Brefeldin A (BFA), a fungal metabolite that inhibits Golgi-to-cell surface traffic²⁹ by blocking some ARF-GEFs and causing release of Golgi-localized ARF^{30,31}. At concentrations of BFA where Golgi disassembly occurs, cell-surface delivery of newly synthesized GPI-AP (CFP-GPI) was inhibited (Fig. 4a). However, endocytosis of fluid phase and GPI-APs was measurably enhanced (Fig. 4b) via the GEEC pathway; endosomes formed during BFA-treatment contain endocytosed FITC-Dex and FR-GPI, but not Tf (see Supplementary information, Fig. S5a). A similar increase in uptake of a fluid-phase marker, HRP, on BFA treatment, has been reported in apical membrane of MDCK cells³². BFA treatment redistributed perinuclear-localized endocytosed Tf into extensive tubular compartments (data not shown) and reduced cell-surface levels of TfR, as previously reported³³, but did not affect the internalization of Tf (Fig. 1a and see Supplementary information, Fig. S5c). Importantly, BFA-mediated increase in uptake via the GEEC pathway was reversed by ARF1^{T31N} expression (Fig. 4c).

Thus, ARF1 is directly required for endocytosis via GEEC pathway, and not indirectly via modulation of exocytic delivery of specific membrane components. These results also demonstrate that ARF1 function in the GEEC pathway is BFA-insensitive, implicating a BFA-resistant GEF in ARF1 activation at the plasma membrane.

ARF1 modulates GEEC pathway via the adaptor ARHGAP10

ARF1 recruits ARHGAP10, a multi-domain protein (M_r , 200K) identified in yeast–two hybrid interaction screen of constitutively active ARF1 and ARF6 (refs 34, 35). ARHGAP10 has a distinct domain (ABD) necessary for binding activated ARF1, and a GAP domain for RhoGTPases (R-G; Fig.5a). ABD encompasses a plekstrin homology (PH) domain, which does not bind to PtdIns, but is essential for ARF binding; the R-G domain possesses a relatively high GAP activity for Cdc42 compared with other Rho GTPases, and mutation of Arg 1183 to alanine in the R-G domain renders it incapable of GAP activity³⁴. When overexpressed, these domains function as dominant-negative inhibitors for the generation of actin-patches on the Golgi³⁴. To determine whether ARHGAP10 could couple the activation of ARF1 with a GAP activity for Cdc42, and in turn affect GPI-AP endocytosis, different domains of this protein were expressed (Fig. 5b). All the truncated domains, with the exception of the mutated RhoGAP domain, were capable of marginal but significant

inhibition of endocytosis via GEECs (Fig. 5b), but not Tf uptake (see Supplementary Information, Fig. S5c).

Overexpression of ARF1^{Q71L}, an isoform of ARF1 deficient in GTP hydrolysis, lead to increased FR–GPI internalization, as well as a more peripheral distribution of FR–GPI endosomes (Fig. 5b, c), suggesting a role for ARF1 in post-endocytic trafficking. Persistent activation of ARF1 was also accompanied by a reduction in Tf uptake (see Supplementary information, Fig. S5c). This could arise due to sequestration of shared GTPase activating proteins (GAPs) for ARF1 and ARF6 that are reported to be involved in clathrin-mediated endocytosis¹⁷. To determine whether ARHGAP10 exerts its effect downstream of activated ARF1, we examined whether coexpression of ARHGAP10 domains would inhibit enhanced FR–GPI internalization induced by ARF1^{Q71L} (Fig. 5b, c). Different domains of ARHGAP10 reversed the ARF1^{Q71L}-induced enhanced FR–GPI uptake to a similar extent (Fig. 5c). The extent of inhibition of uptake was comparable in R-G- and R-G^{R1183A}-domain expressing cells, suggesting that the interaction between ARHGAP10 and Cdc42 was not dependent on the activity of the GAP domain. Taken together with the inhibition observed in the ABD/R-G domain, these data suggest that full-length ARHGAP10 is required as a link between ARF1 and Cdc42.

The inhibition mediated by the ARHGAP10 domains may be explained by sequestration of activated ARF1 and thus inhibition of ARF1, rather than a dominant-negative of ARHGAP10. To determine a role for ARHGAP10 more specifically, endogenous ARHGAP10 was depleted using shRNA. As hamster *ARHGAP10* sequence is unknown, the effects of shRNA were monitored in MEFs, where the uptake of fluid is ARF1 sensitive (Fig. 1b) and the *ARHGAP10* sequence has been determined. The efficacy of shRNA was confirmed by monitoring the depletion of protein levels of an ARHGAP10 fragment when coexpressed with shRNA (Fig. 5e), or by monitoring the effects on actin organization and Golgi morphology as described previously³⁴ (Fig. 5d). In approximately 60% of GFP-expressing cells, the shRNA resulted in alteration in Golgi morphology; fewer cells showed a perturbation of actin organization (approximately 30%). Consistent with this result, expression of shRNA against *ARHGAP10* resulted in approximately 60% of the transfected cells exhibiting a detectable reduction in fluid uptake (Fig. 5f, g). These results implicate ARHGAP10 in uptake via the GEEC pathway, downstream of ARF1 activation, potentially coupling it with GAP activity for Cdc42.

Recruitment of ABD to the plasma membrane is sensitive to ARF1 activation

The involvement of ARF1 in endocytosis at the plasma membrane requires plasma membrane-localized activated ARF1. To observe the distribution of ARF1 at the plasma membrane, total internal reflection fluorescence microscopy (TIRFM) was used to report on distribution of fluorophores in the evanescent field in close proximity (~100 nm for 488nm illumination) to the plasma membrane. TIRFM imaging of live cells expressing low levels of ARF1–GFP revealed relatively stable, punctate structures located at the plasma membrane (Fig. 6a and see Supplementary Information, Movie 1) that were resistant to treatment with BFA (see Supplementary Information, Fig. S5b).

To determine whether the recruitment of the ABD at the plasma membrane depends on ARF1 activation, live cells expressing very low levels of GFP-tagged constructs of different ARHGAP10 domains were imaged using TIRFM (Fig. 6a and see Supplementary Information, Fig. S6a). Low levels of expression provided better contrast of detection in TIRFM and did not affect fluid uptake, therefore acting as non-perturbing reporters. Full-length ARHGAP10 was not detectably expressed in cells³⁴, but similarly to ARF1–GFP, GFP–ABD appeared as relatively stable, punctate structures at the plasma membrane (Fig. 6a). Although GFP–ABD structures were fewer in number than ARF1–GFP, they mimicked both the morphology and distribution of ARF1 puncta. Similar punctuate patterns were observed for ABD/R–G, which can bind to activated ARF1 and Cdc42, but the R–G domain (lacking ABD) was uniformly distributed (see Supplementary information, Fig. S6a). To determine whether ABD is a sensor of ARF1 activation, it was coexpressed with ARF1 shRNA or HA-tagged ARF1^{T31N} (Fig. 6a). In both cases, GFP–ABD was not recruited to the plasma membrane and appeared similar to cytosolic GFP⁹. Furthermore, RFP–ABD punctae colocalized with ARF1–GFP in the TIRFM field (Fig. 6c, d), but not with ARF6–GFP (see Supplementary Information, Fig. S6b–d).

These observations provide evidence for endogenous ARF1 activation and localization at or near the plasma membrane, and support the use of ABD as a reporter for endogenous ARF1 activation. The recruitment of ABD to activated ARF1 sites in the plasma membrane is consistent with the coupling of activated ARF1 to ARHGAP10 in the plasma membrane.

Activated ARF1 is located on early intermediates of the GEEC pathway

If ARF1 activity is required for endocytosis via the GEEC pathway, colocalization of activated ARF1 on nascent endocytic carriers of the GEEC pathway should be observed. For this purpose, cells were pulsed with TMR–Dex for short times (60 s) and imaged. A fraction of fluid-containing endosomes colocalized with GFP–ABD-labelled vesicles and tubules (Fig. 6e) and colocalization was also observed with ARF1–GFP (Fig. 6e).

Newly formed fluid and FR–GPI containing endocytic carriers did not colocalize with coat components such as COPI (known to interact with ARF1 on Golgi and some endosomal membranes³¹), even in the presence of ARF1^{Q71L} (see Supplementary information, Fig. S5d).

ARF1 influences Cdc42 dynamics on plasma membrane

To address the role of ARF1 in regulating Cdc42 dynamics at the plasma membrane, the recruitment of Cdc42 to the plasma membrane was monitored using live-cell TIRFM, both in control cells and after silencing endogenous ARF1 (Fig. 7a). The extent of recruitment, and plasma membrane residence time, of single molecules of Cdc42 are positively influenced by GTP-bound status of Cdc42 (ref. 9). Depletion of ARF1 enhanced both the number of Cdc42 recruitment events and its residence time (Fig. 7a and see Supplementary Information, Movie 2), and formation of cortical spike-like structures (see Supplementary Information, Fig. S2e), consistent with activation of Cdc42 at the plasma membrane^{9,36,37}. Furthermore, similarly to ARF1 silencing, overexpression of a constitutively active form of Cdc42 (Cdc42^{L61}) led to reduction in fluid-phase uptake (Fig. 7b).

To determine whether the coupling of ARF1 activation and Cdc42 dynamics can influence endocytosis via the GEEC pathway, GPI-AP endocytosis was monitored in cells overexpressing ARF1^{Q71L}. Coexpression of Cdc42^{N17} (a GTP-exchange deficient form⁴) or treatment with Toxin B (an inhibitor of Rho GTPases) reverted the activated ARF1^{Q71L}-mediated increase in GEEC endocytosis (Fig. 7c). These results provide evidence that ARF1 is part of the molecular machinery that regulates the GEEC pathway, upstream of Cdc42.

Discussion

ARF1 has been extensively studied in COPI-coated vesicle formation at the Golgi³⁸, and it is also involved in recruiting AP3 and COPI subunits to endosomal membrane buds in PC12 cells^{31,39}. A recent report using a heterologously expressed sensor for activated ARFs detected BFA-insensitive sequential activation of ARF6 followed by ARF1 at sites of phagocytosis⁴⁰.

Our data, using a variety of techniques including RNAi depletion, dominant-negative inhibition and dominant-active activation, support a model (Fig. 7d) wherein activated ARF1 is directly and specifically involved in endocytosis via the Cdc42-regulated GEEC pathway at the cell surface.

There are several lines of evidence that support a role for ARHGAP10 as the downstream effector of activated ARF1 at the plasma membrane, providing the critical GAP-activity necessary for Cdc42 cycling: first, activated ARF1 directly binds to ARHGAP10 (ref. 34) and silencing ARHGAP10 inhibits endocytosis via the GEEC pathway; second, ARF1-binding fragments of ARHGAP10 (ABD) block ARF1^{Q71L}-induced activation of the GEEC pathway, as well as the constitutive operation of this pathway; and third, ABD exhibits a dynamic punctate distribution at the plasma membrane colocalized with ARF1, and maintained by activated ARF1, as depletion of ARF1 or overexpression of ARF1^{T31N} prevents recruitment of the ABD domain. Although ABD serves as a specific reporter for ARF1 on the plasma membrane, ABD is also capable of interacting with both ARF6 and ARF1 on intracellular structures — although much higher expression levels of ARF6 are required for visualizing the colocalization of ABD–RFP and ARF6 (see Supplementary Information, Fig. S6). This difference may arise due to differences in membrane composition at plasma membrane and endomembranes, such that association with ARF1 is more favoured at some regions on the plasma membrane.

These regions could mark the sites where endocytosis via GEECs is initiated by enhancing the local cycling kinetics of Cdc42.

The coupling of ARF1 activation with a Cdc42–GAP activity is supported by the observation that depletion of ARF1 or ARF1^{T31N} expression (data not shown) results in persistently activated Cdc42 at the plasma membrane, as assessed by single-molecule TIRFM. As expression of both GTP-binding and GTPase-deficient mutants of Cdc42 inhibit endocytosis via GEECs, these results support a role for ARF1-activation in dynamic cycling of Cdc42, required for endocytosis via GEECs. Activated Cdc42 is recruited to the plasma membrane and initiates actin polymerization, thereby promoting endocytosis via GEECs in

an actin-independent mechanism⁹. This is reminiscent of ARF1–ARHGAP10 in actin-patch formation at the Golgi³⁴. Likewise, it is possible that the ARF–ARHGAP10 interaction can also aid other endomembrane transport processes, the involvement of these molecular interactions in intracellular trafficking processes is not clear as yet.

The involvement of ARF1 in endocytosis demands a source of activated ARF1 and its effectors (GAPs and GEFs) at the plasma membrane. Our data show that the GEF involved in ARF1 activation is BFA insensitive. Similar observations have been reported in studies on the uptake of FM4-64 in maize root-hair cells⁴¹ and phagocytosis in macrophages⁴⁰, where endocytosis is blocked on overexpression of ARF1^{T31N}, but not by BFA treatment. A recent report has shown that a BFA resistant ARF–GEF, GNL1 is required for selective internalization at the plasma membrane in *Arabidopsis* root-hair cells⁴². The BFA-insensitive GEF could be a member of ARNO–Cytohesin family⁴³. However, expression of deletion mutants of ARNO failed to inhibit GPI-AP's uptake (S.K., unpublished observations), suggesting the use of other GEF(s). Another regulator of dynamin-independent endocytic pathways is the CtBP1–BARS protein, which is reported to aid vesicle fission¹¹. It is interesting that the ARF1-specific GAP protein, ARFGAP1, interacts directly with BARS, and is hypothesized to function as a dynamin counterpart⁴⁴. ARFGAP1 may provide a link for interaction of ARF1 based machinery with CtBP1–BARS.

These studies suggest that endocytosis via the GEEC pathway could be limited by the availability of activated ARF1 at the plasma membrane in a wide variety of cell lines, including a human cell line (S.K., unpublished observations), and support a central role for ARF1 where it is necessary for endocytosis via GEECs, but do not exclude an ancillary role for ARF3 — ARFs have been reported to function in combination in specific trafficking processes²².

Activated ARF1 (detected by ABD-GFP staining) is also found on nascent endocytic structures that contain the fluid phase and have the characteristic tubular morphology of CLICs and GEECs⁵. However, at this time, we cannot determine whether ARF1 is derived directly from the cell surface or independently recruited to CLICs–GEECs, post-internalization. Thus, in addition to its role at the plasma membrane, ARF1 may have other roles in the GEEC pathway. Endocytic carriers stimulated by expression of ARF1^{Q71L} do not colocalize with COPI (β -COP) in fixed cells; ARF1 may recruit other endosomal coats onto GEECs, such as AP3 on endosomes in PC12 cells³⁹ or other molecules¹⁵. Overexpression of ARF1^{Q71L} leads to peripheral distribution of FR endosomes, suggesting a role in post-endocytic trafficking as well.

ARF6 is also thought to regulate a clathrin and dynamin-independent endocytic pathway^{3,16}. As ARF6 depletion or inhibition⁶ has no effect on uptake into GEECs, this argues that the ARF6- and Cdc42-regulated pathways are either distinct processes operating differentially in different cell types, or that ARF6 could modify the ARF1–Cdc42-regulated pathway, post-internalization in some cell types.

In conclusion, we find that multiple proteins, which have a Golgienriched steady-state distribution, are involved in regulating endocytosis via the dynamin-independent pinocytic

(GEEC) pathway. In addition to ARF1, CtBP1–BARS and Cdc42 are both enriched in the Golgi^{11,45}. The involvement of yet another central secretory traffic regulator, ARF1 in endocytosis, raises an interesting possibility that exocytosis and endocytosis may be integrated for maintenance of plasma membrane homeostasis². In addition, our data suggest that this is likely to be accomplished by regulated spatial distribution of distinct ARF1 effectors, and will be a focus of future studies.

Methods

Cell culture, reagents, and plasmids

See Supplementary Information, Methods.

Synthesis of RNAi-resistant ARF1 and shRNA against *ARF6* and *ARHGAP10*

RNAi-resistant ARF1 was generated by using a primer 5′-ATAGGCTTCAACG TGGAAACGGTAGAGTACAAGAACATCAGCTTC-3′, where the nucleotide sequences corresponding to the *ARF1* RNAi sequence used were altered as indicated in bold type. This primer was used to amplify human ARF1–GFP using PCR. The resultant plasmid was sequenced verified before use. *ARF6* shRNA (sequence corresponding to 307–327 nucleotides of human ARF6 coding sequence; 5′-CCAGGAGCTGCACCGCATTAT-3′), was chosen as target sequence. This sequence is conserved in human, mouse and rat *ARF6*. The shRNA against this sequence was ligated into pGSUPER vector, as previously described⁴⁶. A similar procedure was used for generation of *ARHGAP10* shRNA. The sequence chosen was conserved between human and mouse *ARHGAP10* and corresponds to 817–836 in human coding sequence (5′-GTCATTGTGCCTTCTGAGA-3′). For generation of mRFP–ABD, mRFP was obtained from plasmid mRFPpSETb using the primer 5′-ATAGGTACCACCGGTCGCCACCATGGCCTCCTCCGAG-3′. Following the RFP sequence, a 14 bp linker sequence was added such that mRFP sequence is flanked by *AgeI* and *BglII* enzyme sites. EGFP from pEGFPC2–ABD was replaced with mRFP, using these enzyme sites. All of the above mentioned constructs were used after confirmation of sequence following cloning.

Endocytic and exocytic assays and immunofluorescence microscopy

Endocytic and exocytic assays cells were carried out as previously described⁴ with minor modifications, as detailed in the Supplementary Information, Methods.

shRNA transfection and western blotting

shRNA in the pSUPER vector (*ARF1*) was transfected with a fixed ratio of vector carrying the shRNA sequence of interest or pSUPER vector alone (mock) with pEGFP-N1 (3:1, w/w) in 3 cm cover-slip dishes, to ensure cotransfection. Coexpression using this protocol was confirmed by measuring the reduction of protein target levels in GFP-expressing cells by using specific antibodies against the protein target. In all of the endocytic experiments, shRNA was cotransfected with pEGFP-N1 for identification of transfected cells, unless otherwise mentioned. Cells transfected with shRNA directed against *ARF6* in pG-SUPER vectors were identified by GFP coexpression. To biochemically measure protein depletion, cells were plated in 92 mm dishes and cotransfected with shRNA carrying vector or vector

alone (control) with pEGFP-N1. Post-transfection, cells were allowed to grow for 60 h, harvested using trypsin–EDTA, and GFP-positive cells were sorted using FACS-Vantage SE (BD, San Jose, CA). Approximately 30,000 sorted cells from each transfection were lysed and loaded on a 12% SDS–PAGE. Protein estimation was carried out after transfer of proteins on PVDF membranes and the regions corresponding to bands of interest on the membrane were cut and probed using anti-ARF1, anti-ARF6, anti-ARF3 or anti-actin antibodies. The band intensities were sub-sequently quantified.

Imaging, image processing and quantification

Confocal microscopy was carried out on a Zeiss LSM 510 Meta imaging system (63× 1.4 NA; Zeiss, Jena, Germany) or Andor Spinning Disc confocal imaging system (60× 1.42 NA or 100× 1.4 NA, with Ixon EMCCD; Andor Technologies, Belfast, Ireland) using appropriate factory-set filters and dichroics for different fluorophores. Care was taken to avoid fluorophore saturation during acquisition. For quantitative imaging on spinning disc confocal microscope, laser powers and camera gains were maintained constant throughout the experiment. Images acquired using LSM (Zeiss) software or Revolution (Andor) software was converted into TIFF and analysed using Metamorph software. For live imaging, Nikon TE 2000 inverted system equipped with 100× oil objective (NA 1.45) and a cooled CCD cascade camera (Photometrics Inc, Tuscon, AZ) was used. For dual-colour live imaging, cell growth medium was changed to M1 with 0.1% BSA and glucose, and the dishes containing cells were brought to temperature-controlled stage maintained at 37 °C. Images were collected using Metamorph acquisition software.

For quantification of uptake of endocytic tracers, images were obtained using 20×, 0.75 NA objective on widefield microscope (Nikon TE300). The cells from different fields from each dish were defined as regions, and the integrated intensities inside the ‘regions’ were obtained using the ‘region measurement’ application of Metamorph. Average and s.d. of integrated intensities per cell from each dish was determined and plotted as weighted mean of these values, as described in statistical analysis section, unless otherwise stated. The number and intensity of endosomes formed in cells pulsed with TMR–Dex (1 mg ml⁻¹) for 3 min at 37 °C were determined by imaging cells at 20 °C. Images were processed and the endosomes were identified, and total number of endosomes and associated intensity were calculated, as previously described^{4,6}. Briefly, the images were processed for background correction using Metamorph and threshold using Multispot software, such that all the endosomes with intensity above the background were identified. The number of endosomes, area and integrated intensity per endosome were determined per cell using Multispot.

TIRF imaging was carried out exactly as previously described⁹. Cdc42 spots were defined as pixels with intensity values above autofluorescence and correspond to single molecules of Cdc42–GFP according to criterion previously established criterion⁹. Note, bleaching of single GFP fluorophores occurs over a much longer period than measured for the Cdc42–GFP fluorophores. Only spots that make an appearance within the imaging duration (100 ms per frame, 200 frames stream acquisition) were considered for quantification. The residence time of each spot was manually estimated by determining the number of frames it was

visible. The data were binned and expressed as percentage of total number of dynamic spots tracked.

In all cases, images were analysed using Metamorph software and processed for presentation using Adobe Photoshop. Images are displayed at the same contrast-settings for control and treated cells in all display items. The scale bar corresponds to 10 μm , unless otherwise specified.

Statistical analysis

The values plotted are weighted mean, μ_x , obtained from at least two different dishes in each experiment, calculated using the following formula

$$\mu_x = \frac{\sum \frac{n_i \times \bar{X}_i}{\sigma_{X_i}^2}}{\sum \frac{n_i}{\sigma_{X_i}^2}}$$

Equation 1

where i is the number of cover-slip dishes used in an experiment, X_i is the mean of fluorescence intensities determined for cells in a single dish, n_i the number of cells observed per dish, and σ_{X_i} the s.d. in the measurement. The s.e.m. was determined by the following equation,

$$\text{s.e.m} = \left(\sum \frac{\sigma_{X_i}^2}{n_i} \right)^{1/2}$$

Equation 2

unless otherwise specified. Minimum number of cells (n) quantified from an individual dish is indicated in the figure legends. Statistical significance was measured using unpaired, two-tail distribution, Student's *t*-test. Unless specifically mentioned, the *P* values were <0.001 in all cases reported. Each experiment was repeated three or more times with similar results, unless otherwise stated.

Supplementary Material

Refer to Web version on PubMed Central for supplementary material.

Acknowledgments

We thank M. Kalia and B. Srinag for help with biochemistry, H. Krishnamurthy and Wellcome Trust-aided imaging and flow-cytometry facility at NCBS for help with confocal imaging and sorting transfected cells. We are indebted to: G. D. Gupta for making ARF6 shRNA; R. Alexander for *ARF1* RNAi resistant and mRFP-ABD vectors; N. Sabu for ARHGAP10 shRNA; J. Gruenberg for GFP-tagged wild-type ARF1 and ARF1^{T31N} plasmids; S.G. Ferguson for HA-tagged wild-type ARF1, ARF1^{T31N} and ARF1^{Q71L} constructs; P. Chavrier for GFP-ARHGAP10 domains; R. A. Kahn for ARF1, ARF3, ARF4 and ARF5 shRNA plasmids; R. Vishwakarma for fluorescent folate analogues; S. Bourgoin for ARF6-specific antibodies; and R. E. for C₆-LacCer. We thank other members of the Mayor Laboratory and NCBS for generous support and encouragement. S.K. is supported by a pre-doctoral fellowship from Council of Scientific and Industrial Research (Government of India). Work in S.M.'s laboratory is supported by intramural funds from NCBS, and a J. C. Bose fellowship.

References

1. Conner SD, Schmid SL. Regulated portals of entry into the cell. *Nature*. 2003; 422: 37–44. [PubMed: 12621426]
2. Kirkham M, Parton RG. Clathrin-independent endocytosis: new insights into caveolae and non-caveolar lipid raft carriers. *Biochim Biophys Acta*. 2005; 1746: 350–363. [PubMed: 16440447]
3. Mayor S, Pagano RE. Pathways of clathrin-independent endocytosis. *Nature Rev Mol Cell Biol*. 2007; 8: 603–612. [PubMed: 17609668]
4. Sabharanjak S, Sharma P, Parton RG, Mayor S. GPI-anchored proteins are delivered to recycling endosomes via a distinct cdc42-regulated, clathrin-independent pinocytic pathway. *Dev Cell*. 2002; 2: 411–423. [PubMed: 11970892]
5. Kirkham M, et al. Ultrastructural identification of uncoated caveolin-independent early endocytic vehicles. *J Cell Biol*. 2005; 168: 465–476. DOI: 10.1083/jcb.200407078 [PubMed: 15668297]
6. Kalia M, et al. Arf6-independent GPI-anchored protein-enriched early endosomal compartments fuse with sorting endosomes via a Rab5/phosphatidylinositol-3'-kinase-dependent machinery. *Mol Biol Cell*. 2006; 17: 3689–3704. DOI: 10.1091/mbc.E05-10-0980 [PubMed: 16760436]
7. Guha A, Sriram V, Krishnan KS, Mayor S. Shibire mutations reveal distinct dynamin-independent and-dependent endocytic pathways in primary cultures of *Drosophila* hemocytes. *J Cell Sci*. 2003; 116: 3373–3386. [PubMed: 12857788]
8. Gauthier NC, et al. *Helicobacter pylori* VacA cytotoxin: a probe for a clathrin-independent and Cdc42-dependent pinocytic pathway routed to late endosomes. *Mol Biol Cell*. 2005; 16: 4852–4866. DOI: 10.1091/mbc.E05-05-0398 [PubMed: 16055501]
9. Chadda R, et al. Cholesterol-sensitive Cdc42 activation regulates actin polymerization for endocytosis via the GEEC pathway. *Traffic*. 2007; 8: 702–717. [PubMed: 17461795]
10. Glebov OO, Bright NA, Nichols BJ. Flotillin-1 defines a clathrin-independent endocytic pathway in mammalian cells. *Nature Cell Biol*. 2006; 8: 46–54. [PubMed: 16341206]
11. Bonazzi M, et al. CtBP3/BARS drives membrane fission in dynamin-independent transport pathways. *Nature Cell Biol*. 2005; 7: 570–580. [PubMed: 15880102]
12. Sabharanjak S, Mayor S. Folate receptor endocytosis and trafficking. *Adv Drug Deliv Rev*. 2004; 56: 1099–1109. [PubMed: 15094209]
13. D'Souza-Schorey C, Chavrier P. ARF proteins: roles in membrane traffic and beyond. *Nature Rev Mol Cell Biol*. 2006; 7: 347–358. [PubMed: 16633337]
14. Zhang CJ, et al. Expression of a dominant allele of human ARF1 inhibits membrane traffic *in vivo*. *J Cell Biol*. 1994; 124: 289–300. DOI: 10.1083/jcb.124.3.289 [PubMed: 8294513]
15. Nie Z, Hirsch DS, Randazzo PA. Arf and its many interactors. *Curr Opin Cell Biol*. 2003; 15: 396–404. [PubMed: 12892779]
16. Naslavsky N, Weigert R, Donaldson JG. Convergence of non-clathrin- and clathrin-derived endosomes involves Arf6 inactivation and changes in phosphoinositides. *Mol Biol Cell*. 2003; 14: 417–431. DOI: 10.1091/mbc.02-04-0053 [PubMed: 12589044]
17. Tanabe K, et al. A novel GTPase-activating protein for ARF6 directly interacts with clathrin and regulates clathrin-dependent endocytosis. *Mol Biol Cell*. 2005; 16: 1617–1628. DOI: 10.1091/mbc.E04-08-0683 [PubMed: 15659652]
18. Paleotti O, et al. The small G-protein Arf6GTP recruits the AP-2 adaptor complex to membranes. *J Biol Chem*. 2005; 280: 21661–21666. [PubMed: 15802264]
19. Vasudevan C, et al. The distribution and translocation of the G protein ADP-ribosylation factor 1 in live cells is determined by its GTPase activity. *J Cell Sci*. 1998; 111: 1277–1285. [PubMed: 9547306]
20. Dascher C, Balch WE. Dominant inhibitory mutants of ARF1 block endoplasmic reticulum to Golgi transport and trigger disassembly of the Golgi apparatus. *J Biol Chem*. 1994; 269: 1437–1448. [PubMed: 8288610]
21. Lamaze C, et al. Interleukin 2 receptors and detergent-resistant membrane domains define a clathrin-independent endocytic pathway. *Mol Cell*. 2001; 7: 661–671. [PubMed: 11463390]

22. Volpicelli-Daley LA, Li Y, Zhang CJ, Kahn RA. Isoform-selective effects of the depletion of ADP-ribosylation factors 1-5 on membrane traffic. *Mol Biol Cell*. 2005; 16: 4495–4508. DOI: 10.1091/mbc.E04-12-1042 [PubMed: 16030262]
23. Macia E, Chabre M, Franco M. Specificities for the small G proteins ARF1 and ARF6 of the guanine nucleotide exchange factors ARNO and EFA6. *J Biol Chem*. 2001; 276: 24925–24930. [PubMed: 11342560]
24. Shen X, et al. Association of brefeldin A-inhibited guanine nucleotide-exchange protein 2 (BIG2) with recycling endosomes during transferrin uptake. *Proc Natl Acad Sci USA*. 2006; 103: 2635–2640. DOI: 10.1073/pnas.0510599103 [PubMed: 16477018]
25. Choudhury A, Marks DL, Proctor KM, Gould GW, Pagano RE. Regulation of caveolar endocytosis by syntaxin 6-dependent delivery of membrane components to the cell surface. *Nature Cell Biol*. 2006; 8: 317–328. [PubMed: 16565709]
26. Ellis MA, Miedel MT, Guerriero CJ, Weisz OA. ADP-ribosylation factor 1-independent protein sorting and export from the trans-Golgi network. *J Biol Chem*. 2004; 279: 52735–52743. [PubMed: 15459187]
27. Yahara N, Ueda T, Sato K, Nakano A. Multiple roles of Arf1 GTPase in the yeast exocytic and endocytic pathways. *Mol Biol Cell*. 2001; 12: 221–238. DOI: 10.1091/mbc.12.1.221 [PubMed: 11160834]
28. Riezman H. Endocytosis in yeast: several of the yeast secretory mutants are defective in endocytosis. *Cell*. 1985; 40: 1001–1009. [PubMed: 3886157]
29. Doms RW, Russ G, Yewdell JW. Brefeldin A redistributes resident and itinerant Golgi proteins to the endoplasmic reticulum. *J Cell Biol*. 1989; 109: 61–72. DOI: 10.1083/jcb.109.1.61 [PubMed: 2745557]
30. Donaldson JG, Finazzi D, Klausner RD. Brefeldin A inhibits Golgi membrane-catalysed exchange of guanine nucleotide onto ARF protein. *Nature*. 1992; 360: 350–352. [PubMed: 1448151]
31. Gu F, Gruenberg J. ARF1 regulates pH-dependent COP functions in the early endocytic pathway. *J Biol Chem*. 2000; 275: 8154–8160. [PubMed: 10713138]
32. Prydz K, Hansen SH, Sandvig K, van Deurs B. Effects of brefeldin A on endocytosis, transcytosis and transport to the Golgi complex in polarized MDCK cells. *J Cell Biol*. 1992; 119: 259–272. DOI: 10.1083/jcb.119.2.259 [PubMed: 1400572]
33. Shin HW, Morinaga N, Noda M, Nakayama K. BIG2, a guanine nucleotide exchange factor for ADP-ribosylation factors: its localization to recycling endosomes and implication in the endosome integrity. *Mol Biol Cell*. 2004; 15: 5283–5294. DOI: 10.1091/mbc.E04-05-0388 [PubMed: 15385626]
34. Dubois T, et al. Golgi-localized GAP for Cdc42 functions downstream of ARF1 to control Arp2/3 complex and F-actin dynamics. *Nature Cell Biol*. 2005; 7: 353–364. [PubMed: 15793564]
35. Sousa S, et al. ARHGAP10 is necessary for alpha-catenin recruitment at adherens junctions and for Listeria invasion. *Nature Cell Biol*. 2005; 7: 954–960. [PubMed: 16184169]
36. Hall A. Rho GTPases and the actin cytoskeleton. *Science*. 1998; 279: 509–514. [PubMed: 9438836]
37. Yang L, Wang L, Zheng Y. Gene targeting of Cdc42 and Cdc42GAP affirms the critical involvement of Cdc42 in filopodia induction, directed migration, and proliferation in primary mouse embryonic fibroblasts. *Mol Biol Cell*. 2006; 17: 4675–4685. DOI: 10.1091/mbc.E06-05-0466 [PubMed: 16914516]
38. Spang A. ARF1 regulatory factors and COPI vesicle formation. *Curr Opin Cell Biol*. 2002; 14: 423–427. [PubMed: 12383792]
39. Faundez V, Horng JT, Kelly RB. A function for the AP3 coat complex in synaptic vesicle formation from endosomes. *Cell*. 1998; 93: 423–432. [PubMed: 9590176]
40. Beemiller P, Hoppe AD, Swanson JA. A phosphatidylinositol-3-kinase-dependent signal transition regulates ARF1 and ARF6 during Fcγ receptor-mediated phagocytosis. *PLoS Biol*. 2006; 4 e162 doi: 10.1371/journal.pbio.0040162 [PubMed: 16669702]
41. Xu J, Scheres B. Dissection of Arabidopsis ADP-RIBOSYLATION FACTOR 1 function in epidermal cell polarity. *Plant Cell*. 2005; 17: 525–536. DOI: 10.1105/tpc.104.028449 [PubMed: 15659621]

42. Teh OK, Moore I. An Arf-GEF acting at the Golgi and in selective endocytosis in polarized plant cells. *Nature*. 2007; 448: 493–496. [PubMed: 17653191]
43. Chardin P, et al. A human exchange factor for Arf contains Sec7- and pleckstrin homology domains. *Nature*. 1996; 384: 481–484. [PubMed: 8945478]
44. Yang JS, et al. Key components of the fission machinery are interchangeable. *Nature Cell Biol*. 2006; 8: 1376–1382. [PubMed: 17086176]
45. Erickson JW, Zhang C, Kahn RA, Evans T, Cerione RA. Mammalian Cdc42 is a brefeldin A-sensitive component of the Golgi apparatus. *J Biol Chem*. 1996; 271: 26850–26854. [PubMed: 8900167]
46. Kojima S, Vignjevic D, Borisy GG. Improved silencing vector co-expressing GFP and small hairpin RNA. *Biotechniques*. 2004; 36: 74–79. [PubMed: 14740488]

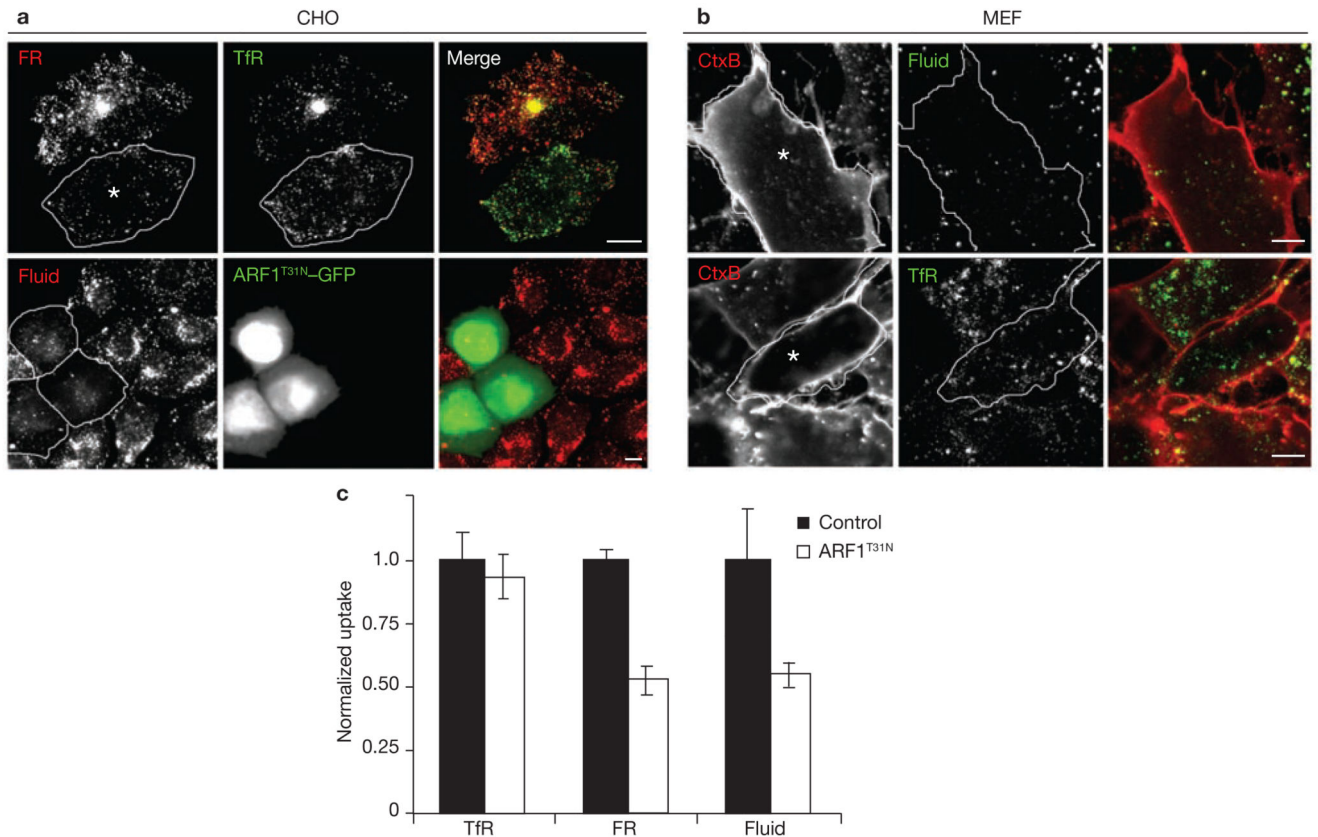


Figure 1. GDP-exchange deficient ARF1 inhibits uptake of GPI-APs and the fluid-phase.

(a) IA2.2 cells (CHO cells expressing FR-GPI (FR) and human TfR) were transiently transfected with ARF1^{T31N}-GFP (outlined cells) for 18 h, and pulsed with Alexa⁵⁶⁸Mov19 Fabs and Alexa⁶⁴⁷ Tf (upper panels) or TMR-Dex (lower panels) for 10 min and processed for imaging. Images of internalized FR (red), TfR (green) and the fluid-phase (Fluid; red), are shown in grey-scale and colour merge. In transfected IA2.2 cells, the intracellular distribution of TfR containing perinuclear recycling compartment (REC) is altered, but Tf-uptake is unaffected. (b) MEFs transfected with ARF1^{T31N}-GFP for 20 h, were pulsed with labelled probes for 5 min, fixed and imaged on a confocal microscope. Grey-scale and colour merge images of internalized Cy5-CTxB (CTx; red) with TMR-Dex (lower panel; green) or Alexa⁵⁶⁸Tf (upper panel; green) from a single confocal section are shown (transfected cells are outlined). In transfected cells, uptake of CTxB is blocked and fluid uptake is significantly reduced while TfR-uptake is unaffected. (c) Histogram showing uptake of TfR, FR-GPI (normalized to surface receptor expression level) and fluid-phase in ARF1^{T31N} transfected cells plotted as a ratio to corresponding uptake measured in control cells. The error bars represent the weighted mean of fluorescence intensities \pm s.e.m. ($n = 61, 68, 100, 77, 63, 68$; asterisks represent the cells transfected with ARF1^{T31N}). The scale bars in **a** and **b** represent 10 μ m.

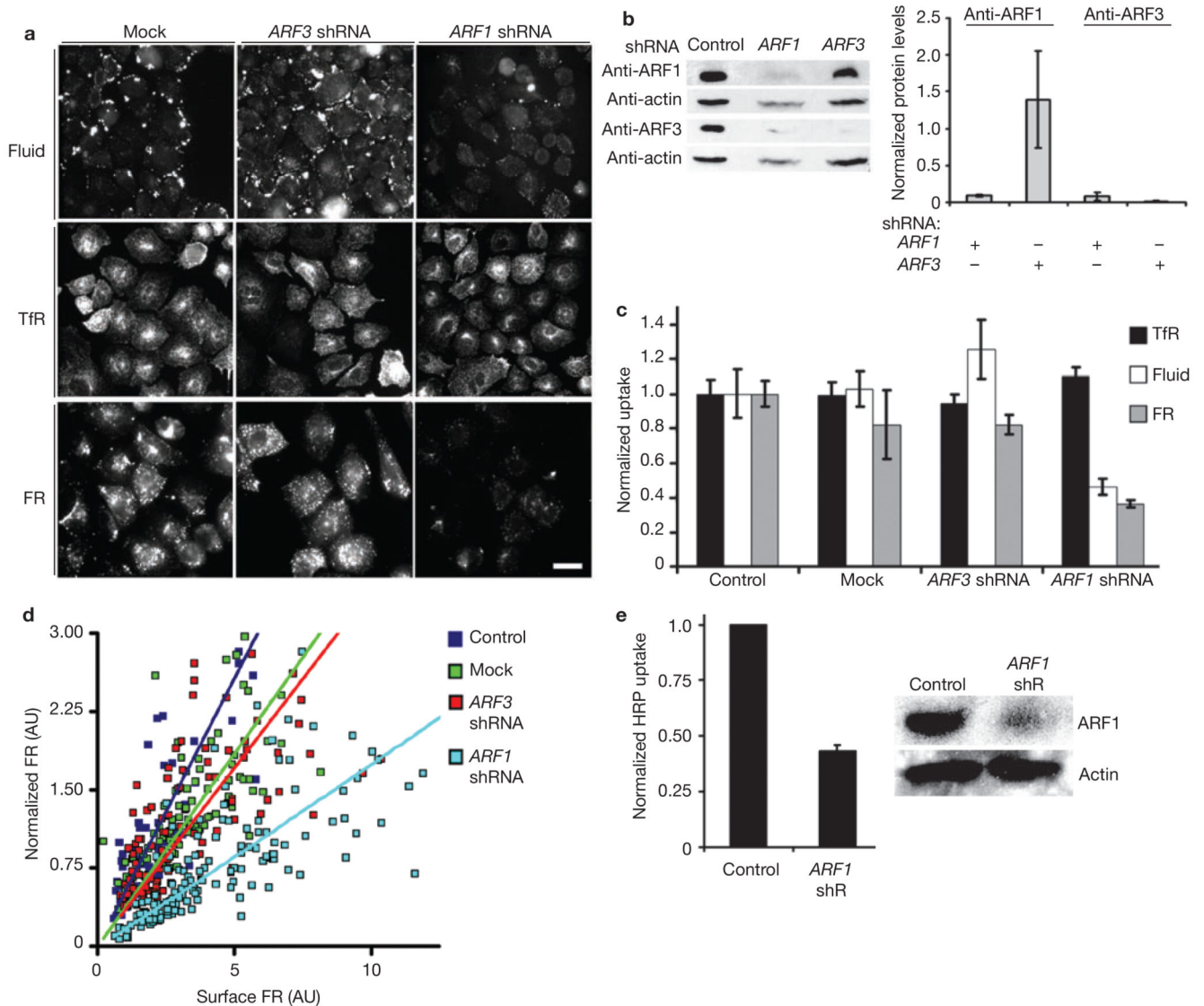


Figure 2. GEEC pathway is inhibited by depletion of ARF1 protein.

(a, b) IA2.2 cells cotransfected with pEGFP-N1 and the indicated shRNA or pSUPER vector (mock) were monitored for endocytosis as described in Fig. 1 (a) or harvested for western blotting (b). The histogram (b) shows the average (\pm s. d.) of data from three experiments of normalized levels of ARF1 and ARF3 in cells sorted for GFP fluorescence, where the amount of ARF protein as detected on western blots is normalized to the actin level per lane, and expressed as a ratio with respect to the value obtained in mock-transfected sample. (c) Histogram showing quantification of endocytosed probes in the cells expressing GFP, where each bar represents endocytosed fluorescence intensity (normalized surface receptor expression, TfR and FR) expressed relative to that measured in mock-transfected cells. Values plotted are weighted mean \pm s.e.m. ($n = 126, 116, 91, 95, 96, 103, 92, 90, 113, 100, 110$). (d) Scatter graph (and trend lines) showing variation of endocytosed PLR (FR–GPI) probe fluorescence intensities versus surface FR–GPI levels in individual cells transfected with indicated shRNA, from 80 cells per condition. FR–GPI uptake in cells was measured

by monitoring endocytosed PLR as above, and surface levels of FR–GPI were quantified by measuring cell surface Cy5–Mov19 binding capacity. **(e)** Histogram showing the amount of endocytosed HRP in cells transfected with vector alone (control) or *ARF1* shRNA. Each bar represents the average of HRP activity normalized to the control, from two representative experiments \pm s.d. Western blot shows the extent of reduction in ARF1 levels in cells taken for HRP uptake assays. The scale bar in **a** represents 20 μ m.

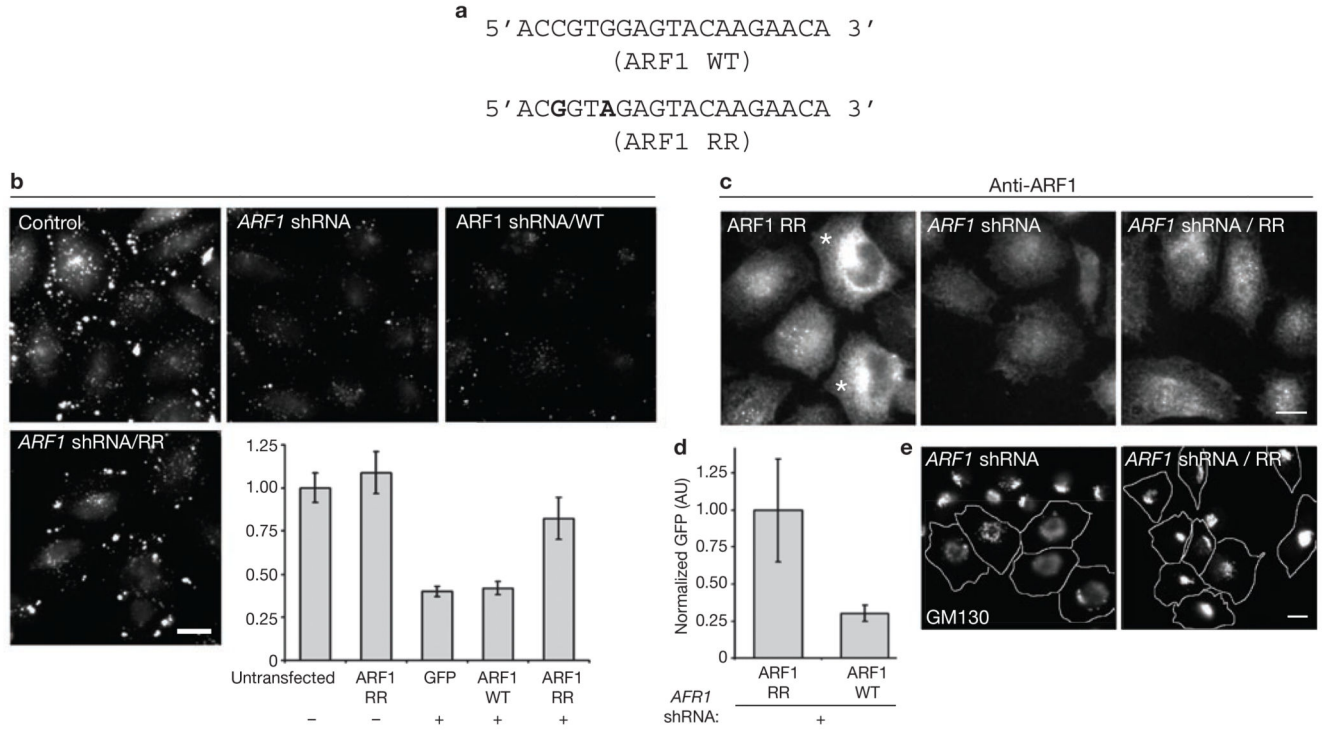


Figure 3. RNAi-resistant ARF1 reverts shRNA-mediated inhibition of the GEEC pathway.

(a) Silent nucleotide substitutions in primers employed to create *ARF1* RNAi-resistant (RR) form are highlighted in bold-type, with respect to positions in wild-type (WT) ARF1. (b) IA2.2 cells transfected with ARF1 RR–GFP (control), *ARF1* shRNA alone, or *ARF1* shRNA and ARF1 WT–GFP (*ARF1* shRNA/WT), or *ARF1* shRNA and ARF1 RR–GFP (*ARF1* shRNA/RR), were assessed for endocytosis of the fluid phase 60 h post-transfection. The histogram shows the quantification of fluid uptake in the indicated GFP-expressing cells. The error bars represent weighted mean, normalized to untransfected (control) cells, \pm s.e.m. ($n = 89, 81, 109, 84, 97$). This experiment was repeated twice with similar results. (c) Cells transfected with indicated expression vectors for 60 h were fixed and processed for immunofluorescence microscopy to detect ARF1 levels. ARF1 RR–GFP overexpressing cells are marked with an asterisk. Note that coexpression of ARF1 RR–GFP with shRNA restores the ARF1-antibody staining levels comparable to unmarked cells in ARF1 RR panel. (d) Histogram representing the average GFP-fluorescence intensity in cells cotransfected with *ARF1* shRNA together with ARF1 WT–GFP or ARF1 RR–GFP, normalized to GFP fluorescence levels in ARF1 RR–GFP transfected cells. The error bars represent weighted mean of GFP intensities detected in individual cells (arbitrary units, AU) \pm s.e.m. ($n = 120, 91$). This experiment was repeated twice with similar results. (e) Overexpression of ARF1 RR–GFP in *ARF1* shRNA transfected cells restores typical Golgi morphology as assessed by monitoring GM130 antibody staining pattern. Approximately 70% of cells transfected with *ARF1* shRNA exhibited a disrupted Golgi pattern. Note GM130 staining in the shRNA-expressing outlined cell versus surrounding untransfected cells. In contrast, only approximately 30% of cells exhibit this phenotype in

cells cotransfected with ARF1 RR–GFP ($n = 80$). The scale bars in **b**, **c** and **e** represent 10 μm .

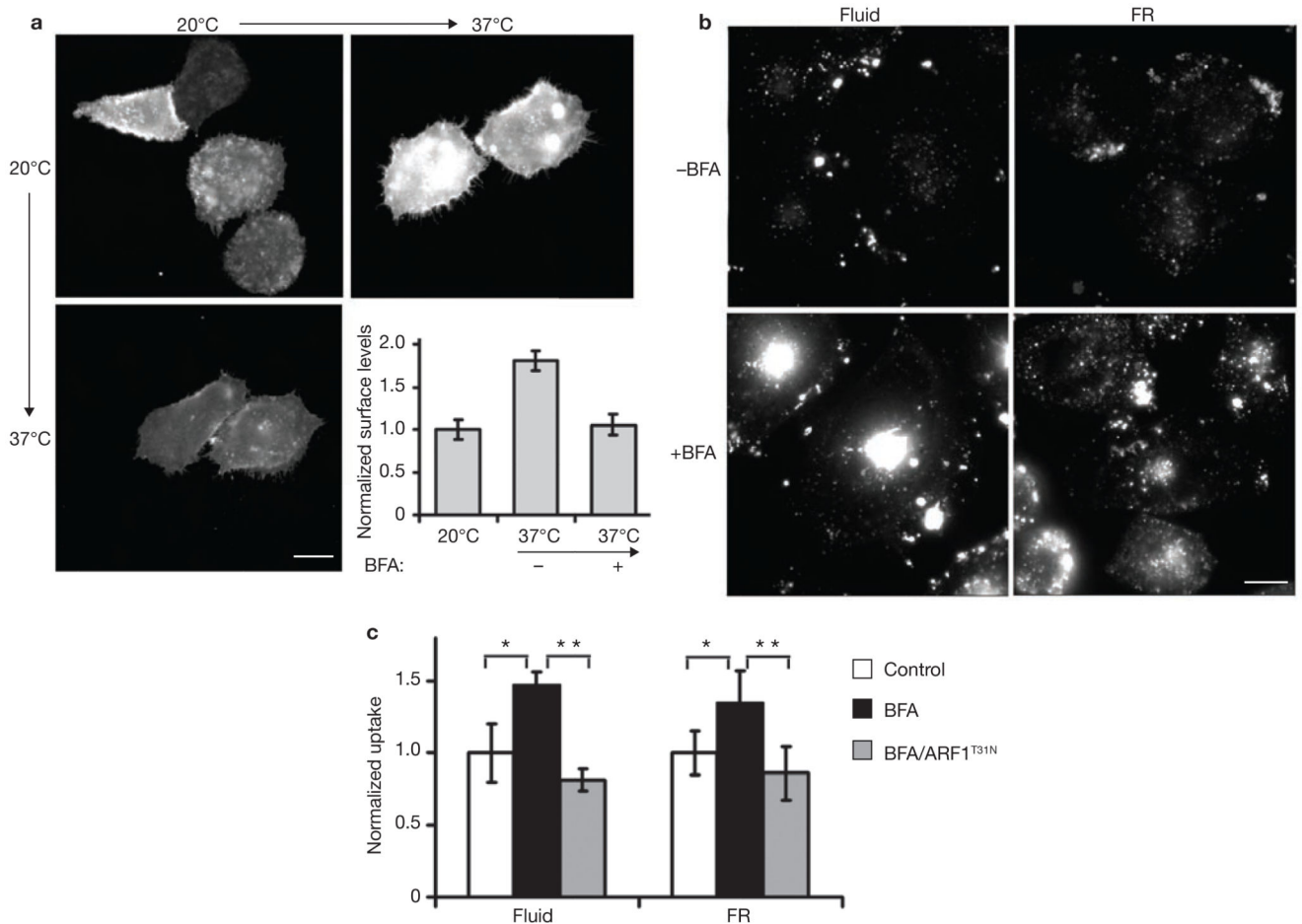


Figure 4. Brefeldin A inhibits surface delivery of GPI-APs, but enhances endocytosis via the GEEC pathway.

(a) CHO cells transiently transfected with CFP-GPI were grown at 20 °C for 16 h and then shifted to 37 °C in presence (+BFA, 20 $\mu\text{g ml}^{-1}$) or absence of Brefeldin A (-BFA) for 1 h. Surface levels of CFP-GPI, monitored by labelling cells with anti-CFP at 4 °C, shows that BFA-treatment blocks exocytic delivery of CFP-GPI. The histogram shows anti-CFP antibody fluorescence at the surface of cells, normalized to total CFP-GPI expression per cell, and plotted as a ratio to the cell surface levels measured at 20 °C. The error bars represent weighted mean \pm s.e.m. ($n = 56, 40, 55$). (b) IA2.2 cells, treated with BFA (20 $\mu\text{g ml}^{-1}$ for 1 h at 37 °C) were assayed for FR-GPI and the fluid-phase uptake as described in Fig. 1. In BFA-treated cells, fluid-phase and FR-GPI uptake is enhanced. (c) Histogram showing quantification of fluorescence of endocytosed probes (normalized to FR-GPI expression at the surface for FR-GPI uptake) in cells treated with BFA in the presence or absence of ARF1^{T31N} transfection, represented as the ratio of uptake to that observed in untreated cells (control). The error bars represents weighted mean \pm s.e.m. ($n = 98, 139, 71$ for fluid and 103, 112, 64 for FR). The single and double asterisks represent P values (<0.002) from the indicated comparisons. The scale bars in **a** and **b** represent 10 μm .

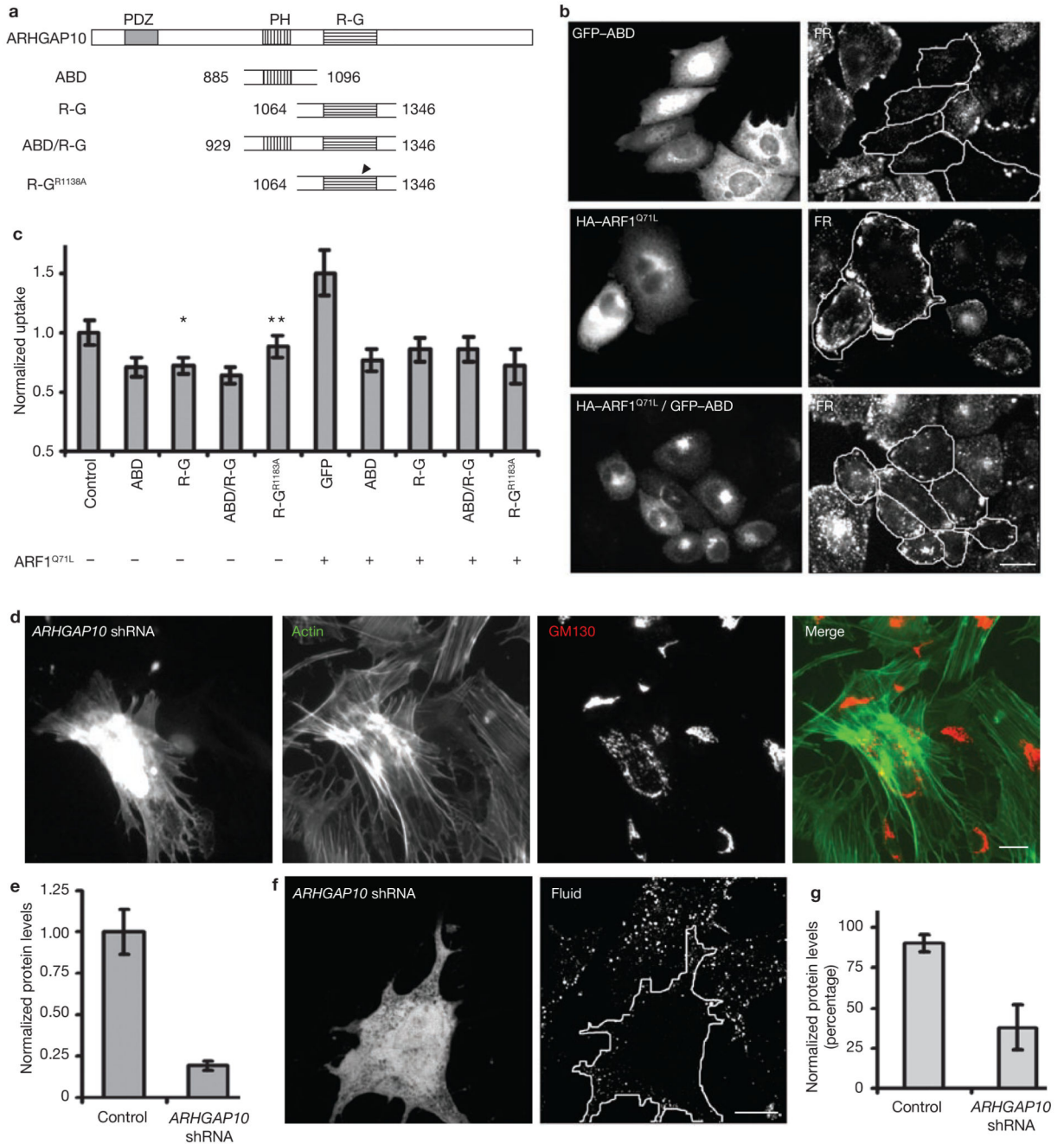


Figure 5. ARF1 functions via ARHGAP10.

(a) Deletion constructs of ARHGAP10 with different domains. ARF binding domain, ABD; RhoGAP domain, R-G; ABD and R-G domain, ABD/R-G; R-G domain mutated for GAP activity, R-G^{R1183A}. (b) IA2.2 cells transfected with either singly with GFP-ABD, HA-ARF1^{Q71L} or with both constructs were assayed for endocytosis of FR-GPI. Expression of GFP-ABD reduces, whereas ARF1^{Q71L} expression enhances FR-GPI uptake. Endocytosed FR-GPI is more peripherally distributed in ARF1^{Q71L}-expressing cells. Coexpression of both proteins (outlined cells) shows that GFP-ABD expression antagonizes ARF1^{Q71L}.

mediated endocytic enhancement. (c) Histogram showing quantification of internalized FR–GPI in cells expressing the indicated combination of constructs, normalized to that measured in GFP-transfected cells. The error bars represent weighted mean \pm s.e.m. ($n = 66, 49, 54, 57, 50, 50, 44, 56, 49$). The single asterisk and the double asterisk represent P values 0.01, and 0.2, respectively. (d) MEFs transfected with *ARHGAP10* shRNA for 72 h were fixed and stained for actin organization and Golgi morphology (GM130). Note that in transfected cells, the actin distribution is altered and Golgi is dispersed. This F-actin reorganization is observed in approximately 30% of transfected cells and change in Golgi morphology is observed in approximately 60% cells. (e) Histogram showing levels of anti-V5 antibody staining in V5-tagged *ARHGAP10* N-terminal domain coexpressed with eGFP-N1 (control) or *ARHGAP10* shRNA in CHO cells. The error bars represent weighted mean of average of V5 intensities per cell \pm s.e.m. ($n = 97, 82$). (f) MEFs expressing *ARHGAP10* shRNA (outlined, green in merge) exhibit a reduction in fluid-phase uptake (outlined, right panel) compared with surrounding untransfected cells. Images are single confocal plane representing either transfection marker or internalized fluid. (g) Histogram showing the percentage of cells (MEFs) that exhibit a normal fluid-phase uptake in cells expressing GFP alone (control) or *ARHGAP10* shRNA, when compared to untransfected cells. The error bars represent average of data from three independent experiments \pm s.d. ($n = 35, 56$). The scale bars represent 20 μm .

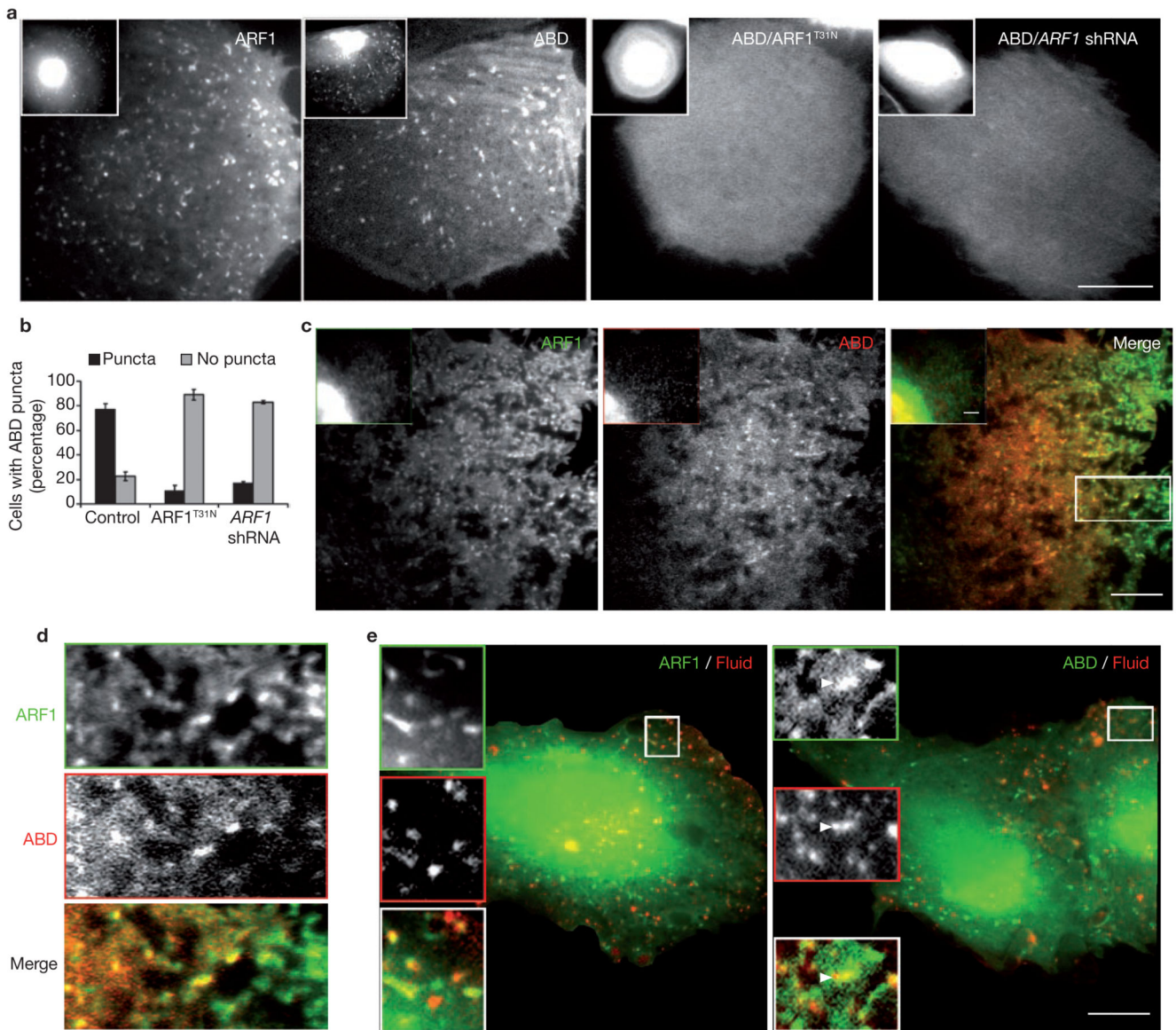


Figure 6. Activated ARF1 is located at the plasma membrane and on fluid-containing nascent endosomes.

(a) IA2.2 cells transfected with ARF1–GFP and GFP–ABD expression vectors as indicated were sequentially imaged using TIRF and wide-field illumination. ARF1–GFP and GFP–ABD appear enriched on the Golgi in the wide-field (inset), whereas in the same cells distinct punctate foci of these proteins are visible in the TIRF field. Cotransfection of cells with HA–ARF1^{T31N} and *ARF1* shRNA removes these foci from the plasma membrane. (b) Histogram showing the fraction of GFP–ABD transfected cells with punctate distribution on cotransfection with ARF1^{T31N} or *ARF1* shRNA. The error bars represent weighted mean \pm s.e.m. ($n = 45, 36, 42$). (c) IA2.2 cells transfected with ARF1–GFP and RFP–ABD were imaged live using sequential TIRF illumination. The delay between acquisition of ARF1 and ABD images is 200 ms. Note that in merge of ARF1 and ABD images, all the ABD puncta colocalize with ARF1. A portion of merge (box) is magnified in e. (e) IA2.2 cells transfected

with ARF1–GFP (left, green) or GFP–ABD (right, green) were pulsed with TMR–Dex (Fluid, red) for 40 s at 37 °C, washed, fixed and imaged. Insets show a magnified view of the region demarcated with a square, where there is extensive colocalization of the two colours. The scale bars in **a**, **d** and **e** represent 10 μ m.

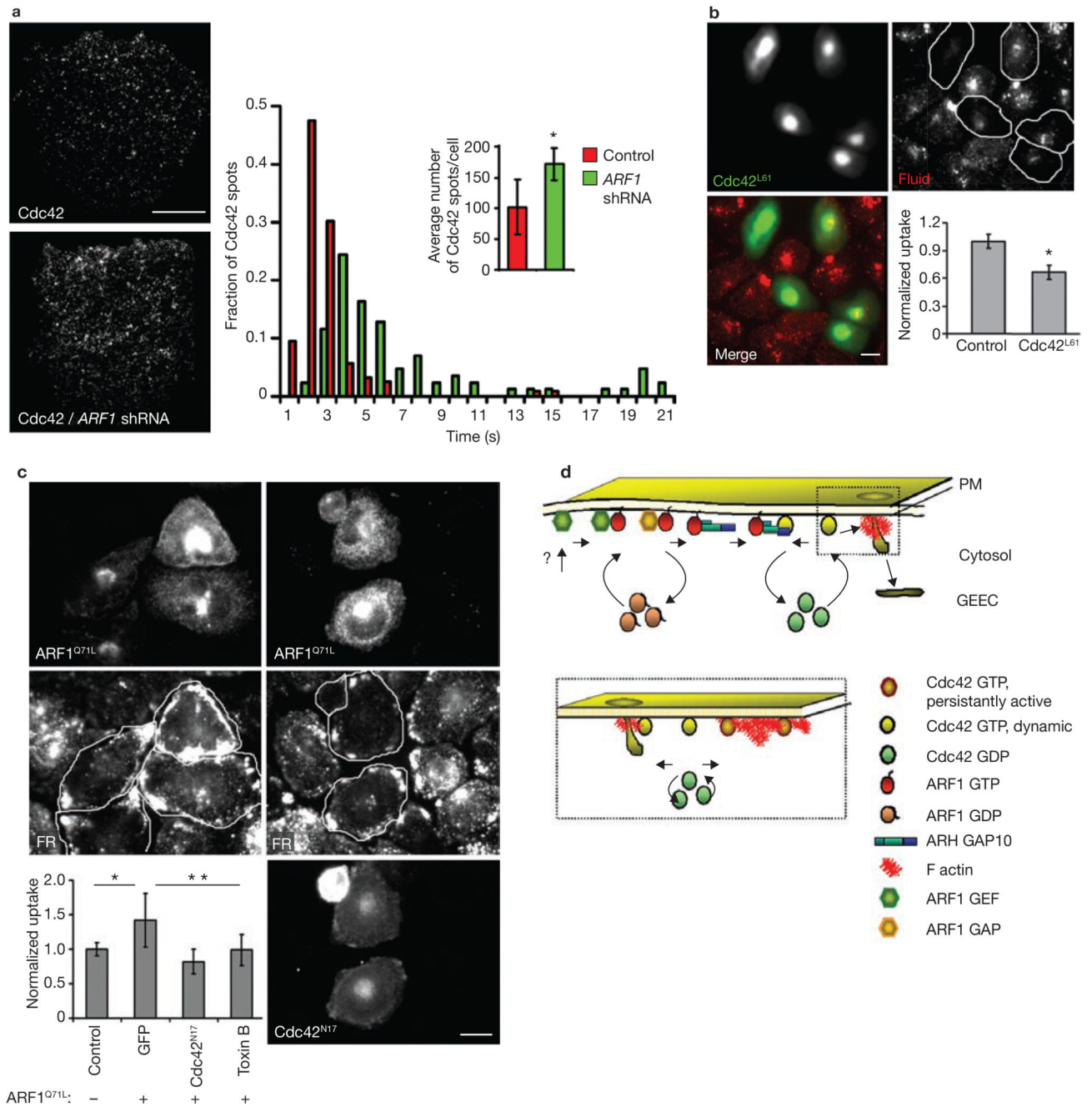


Figure 7. ARF1 activation couples to Cdc42 dynamics at plasma membrane.

(a) IA2.2 cells expressing Cdc42–GFP, without or with cotransfection of *ARF1* shRNA were imaged at 37 °C under TIRF illumination to visualize distribution of single molecules of Cdc42 at the plasma membrane. The histogram shows that the mean residence time of Cdc42 (indicated by arrows) and the average number of molecules (\pm s.d.) shown in the inset, increase in *ARF1* shRNA transfected cells. Data are from one experiment out of two with similar results, where 12 cells in each condition were analysed. The asterisk indicates $P < 0.006$. (b) IA2.2 cells transfected with GFP–Cdc42^{L61} (green in merge) were

pulsed with TMR–Dex (red in merge), fixed and imaged. The histogram shows the uptake of TMR–Dex in cells expressing GFP–Cdc42^{L61} normalized to untransfected cells from a single experiment, repeated twice with similar results. The error bars represent weighted mean \pm s.e.m. ($n = 50, 58$). The asterisk represents $P = 0.002$. (c) IA2.2 cells transfected with HA–ARF1^{Q71L} either alone or with Cdc42^{N17} were assayed for FR–GPI uptake (FR), and processed for detection of HA–ARF1^{Q71L} and GFP. The histogram shows quantification of endocytosed Alexa568–Mov19 Fab fluorescence (normalized to surface FR–GPI levels) in cells expressing ARF1^{Q71L}, cotransfected with GFP–Cdc42N17, or treated with Toxin B (1 $\mu\text{g ml}^{-1}$ for 60 min), plotted as a ratio to uptake measured in untransfected (control) cells. The error bars represent weighted mean \pm s.e.m. ($n = 60, 78, 73, 79$). The single and double asterisks represent $P = 0.003$ for the indicated comparisons. (d) In a model for ARF1-dependent regulation of endocytosis via GEEC pathway, ARF1 activity is governed by a BFA-resistant GEF and a GAP of unknown identity (?). Activated ARF1 recruits ARHGAP10 to function as a RhoGAP for Cdc42, resulting in inactivation and release of Cdc42 into cytosol. Activated Cdc42 regulates dynamic actin polymerization that leads to formation of endosomes via the GEEC pathway. However, persistent activation of Cdc42 (due to constitutively activated Cdc42 or loss of ARHGAP10-based RhoGAP activity) leads to a different type of actin architecture (see box), incompatible with endocytosis via the GEEC pathway. The scale bars in **a**, **b** and **c** represent 10 μm .

Table 1

	ShRNA target	Sequence (5'-3')
1.	ARF1 ³	ACCGTGGAGTACAAGAACA
2.	ARF1 ³	TGACAGAGAGCGTGTGAAC
3.	ARF3 ³	ACAGGATCTGCCTAATGCT
4.	ARF4 ³	TCTGGTAGATGAATTGAGA
5.	ARF5 ³	TCTGCTGATGAACTCCAGA
6.	ARF6 (this study)	CCAGGAGCTGCACCGCATTAT
7.	ARHGAP10 (this study)	GTCATTGTGCCTTCTGAGA